JOURNAL OF GUIDANCE, CONTROL, AND DYNAMICS
Vol. 22, No. 1, January–February 1999

Modeling and Control of a Flexible Structure Incorporating Inertial Slip-Stick Actuators

A. P. Darby*
University of Oxford, Oxford, England OX1 3PJ, United Kingdom
and
S. Pellegrino†
University of Cambridge, Cambridge, England CB2 1PZ, United Kingdom

Shape and vibration control of a linear flexible structure by means of a new type of inertial slip-stick actuator are investigated. A nonlinear model representing the interaction between the structure and a six-degree-of-freedom Stewart platform system containing six actuators is derived, and closed-loop stability and performance of the controlled systems are investigated. A linearized model is also derived for design purposes. Quasistatic alignment of a payload attached to the platform is solved simply by using a proportional controller based on a linear kinematic model. The stability of this controller is examined using a dynamic model of the complete system and is validated experimentally by introducing random thermal elongations of several structural members. Vibration control is solved using an H_∞ loop-shaping controller and, although its performance is found to be less satisfactory than desired, the nonlinear model gives good predictions of the performance and stability of the closed-loop system.

Introduction

OVER the last 20 years or so, there has been an increase in the number of optical structures being sent into orbit to perform scientific observations outside of Earth's atmosphere. These structures, such as space telescopes and optical interferometers, have been increasing in size, yet higher quality images are required. Disturbances in the form of quasistatic thermal distortions or initial structural deformations reduce the achievable resolution, and vibrations caused by momentum wheels or thermal shock cause blurring. The relative alignment of optical instruments must be maintained over tens of meters despite these disturbances and, although in the past these effects have been controlled through passive means, active control is becoming necessary to meet more stringent demands. The introduction into a structure of actuators and sensors connected via closed-loop feedback controllers allows the physical characteristics of the structure to be altered in a desirable manner.

This paper describes a system that provides six-degree-of-freedom (6DOF) alignment correction of a payload mounted at the tip of a flexible structure, subject to dynamic and quasistatic disturbances, via a Stewart platform arrangement. The six legs of the platform are formed by a new type of inertial slip-stick actuator. Nonlinearities associated with the actuator are modeled, allowing the interaction between the Stewart platform and the structure to be described. Controllers capable of reducing quasistatic and dynamic disturbances are designed, and their performance is assessed.

An advantage of the Stewart platform is that the minimum number of actuators are used, i.e., six, to provide motion in 6DOFs (three mutually perpendicular translations and their corresponding rotations) in a statically determinate configuration. This is one of the reasons why Stewart platforms are widely used for robot manipulators and flight simulators, which was the original motivation behind their design.[1] The Stewart platform module can be attached to a flexible structure to provide independent articulation between subsystems, allowing correction for both quasistatic disturbances and vibrations.

Stewart platform systems have been proposed for both 6DOF vibration control and shape control strategies. Geng and Haynes[2] developed a multi-DOF (MDOF) Stewart platform arrangement using Terfenol-D Magnetostrictive actuators for vibration isolation and control purposes. To circumvent the problems encountered in some linear quadratic Gaussian (LQG) optimal controller designs, a robust adaptive filter algorithm was developed. A cubic configuration was used to simplify the kinematics of the system. A similar isolator, incorporating soft voice-coil actuators, was also examined.[3] However, both systems were tested in rather idealized conditions, connected to shaking tables rather than flexible structures.

Shape control systems using long-stroke actuators have also taken advantage of the Stewart platform arrangement. Several sets of actuators can be arranged to form a variable geometry truss providing rigid-body articulation for use as space cranes and robot manipulators. Tanaka and Hanahara[4] have investigated the use of such an arrangement to form a helical mast. The kinematics of each module are used incrementally to establish the position of the tip of the mast.

The work presented in this paper aims to provide an intermediate solution that is able to correct for misalignment of a payload in 6DOFs for both low-frequency vibrations and quasistatic disturbances. A new type of long-stroke, high-resolution actuator was developed for performing these tasks. However, the behavior of these actuators is inherently nonlinear, and this nonlinearity has to be considered when modeling the interaction between the actuators and the rest of the structure.

Active Module Design

To be capable of controlling both quasistatic and dynamic disturbances at the tip of a structure, the actuators must be able to perform large, slow changes in length, as well as more rapid, smaller amplitude motions. An inertial slip-stick actuator, shown in Fig. 1, has been developed to meet these requirements.[5]

The actuator consists of an inner sliding section held by friction within an outer holder. For motion of the sliding section to occur, a force greater than the friction force must be applied. This is achieved through the acceleration of an inertial mass connected to the sliding section via a piezoelectric element. By applying a discontinuous voltage waveform to the piezoelectric element, large accelerations of the inertial mass are caused, resulting in a periodic impulse force being applied to the sliding section. This stick-slip motion of the sliding section moves the actuator in a series of small steps, which can be approximated as a linear motion if the actuator is driven at high frequencies (2000 Hz). The actuator can achieve velocities of up to 9 mm/s with maximum changes in length of 25 mm while maintaining submicrometer resolution.

Figure 2 shows the measured velocity output/voltage input relationship of an actuator, under various loads F. The voltage

Received Nov. 12, 1996; revision received July 12, 1998; accepted for publication July 27, 1998.

*Leverhulme Research Fellow, Department of Engineering Science, Parks Road.

†Reader in Structural Engineering, Department of Engineering, Trumpington Street. Senior Member AIAA.

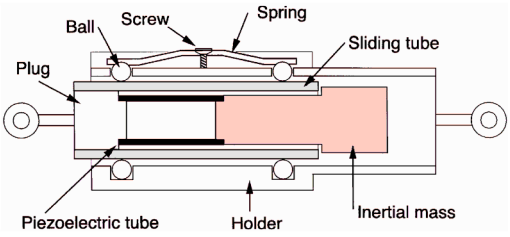

Fig. 1 Inertial stick-slip actuator.

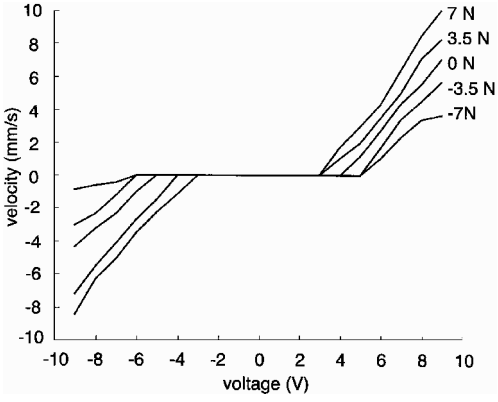

Fig. 2 Actuator velocity-voltage relationship for different forces F.

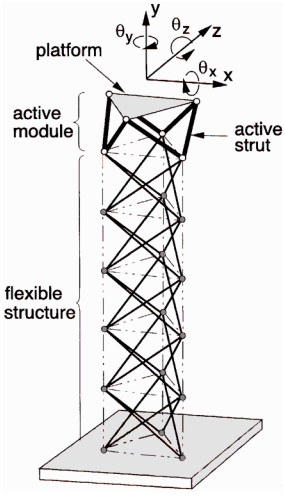

Fig. 3 Flexible structure with active module.

represents the amplitude of the input waveform, which is subsequently factored by a constant gain of 45. By fitting the experimental data with two planes (one for positive velocities, one for negative), an approximate expression for force in terms of velocity $\dot{\delta}$ and voltage v is given by

$$F = a\dot{\delta} + bv + n \tag{1}$$

where the coefficients a, b, and n change depending on the sign of $\dot{\delta}$.

Six of these actuators are incorporated into a Stewart platform arrangement (Fig. 3). The relationship between the 6DOF generalized displacements $\boldsymbol{y}$ of the centroid of the platform and the changes in length of the actuators $\boldsymbol{\delta}$ can be expressed by a 6×6 Jacobian matrix $\boldsymbol{J}$:

$$\boldsymbol{y} = \boldsymbol{J}\boldsymbol{\delta} \tag{2}$$

In general, the entries in the Jacobian matrix are nonlinear because they are geometry dependent. However, assuming that platform motion remains small, i.e., $\delta \ll L$, where L is the initial length of the actuator, $\boldsymbol{J}$ becomes approximately constant because geometrical changes are insignificant.

The active module formed by the actuators can be added to the tip of a flexible structure to maintain alignment between the payload mounted on top of the module and the base of the structure. This may represent a flexible appendage carrying an optical instrument to be kept in alignment with a collector on the body of the spacecraft. Rigid-body motion of the spacecraft and flexibility of the connection to the spacecraft have been ignored, but could be incorporated into the model.

For the experimental work reported in this paper, a fully deployed pantographic deployable mast[6] was chosen to represent a typical flexible appendage. The complete system is shown in Fig. 3. The mast is approximately 1.5 m tall, and the active module adds another 0.3 m to the height. The complete system has a fundamental natural frequency of approximately 4 Hz, corresponding to the first bending mode. The first torsional mode occurs at approximately 20 Hz and the second bending mode at 29 Hz. These modes are contained within the proposed controller bandwidth.

It is assumed that the structure to be controlled can be adequately represented by a linear model (such as that given by finite element analysis) and that the nonlinearities of the system stem from the actuators. Hence, the equation representing the dynamics of the system is given by

$$\boldsymbol{M}\ddot{\boldsymbol{x}} + \boldsymbol{D}\dot{\boldsymbol{x}} + \boldsymbol{K}\boldsymbol{x} = \boldsymbol{C}_1\boldsymbol{f}_u + \boldsymbol{C}_2\boldsymbol{f}_{\mathbf{dist}} \tag{3}$$

where $\boldsymbol{M}$, $\boldsymbol{D}$, and $\boldsymbol{K}$ are the mass, damping, and stiffness matrices, respectively, $\boldsymbol{x}$ is a vector of generalized displacements, $\boldsymbol{f}_u$ is a vector of generalized control forces, and $\boldsymbol{f}_{\mathbf{dist}}$ is a vector of external disturbance forces with corresponding influence matrices $\boldsymbol{C}_1$ and $\boldsymbol{C}_2$. The following sections derive an expression for $\boldsymbol{C}_1\boldsymbol{f}_u$ in terms of the actuator input v.

Simple Two-Degree-of-Freedom System

The approach to the derivation of the MDOF interaction model is most easily understood through the example of a simple two-degree-of-freedom (2DOF) system with a single actuator. The system shown in Fig. 4a consists of two masses M_s and M_p, a spring k_s and damper d_s mounted in parallel, and an actuator. The spring, damper, and mass system associated with the mass M_s represents a simple flexible structure with a single DOF x_s, and the mass M_p represents a payload with a single DOF x_p.

The actuator is assumed to be a rigid element. Hence, x_p can be related to x_s through the equation

$$x_p = x_s + \delta \tag{4}$$

where δ is the change in length of the actuator due to a control input.

The system can be represented by the two subsystems shown in Fig. 4b where F is the force in the actuator. The equations of motion for the two systems are given by Eq. (3) and Newton's second law of motion, respectively,

$$M_s\ddot{x}_s + d_s\dot{x}_s + k_s x_s = -F \tag{5}$$

$$F = M_p(\ddot{x}_s + \ddot{\delta}) \tag{6}$$

To have voltage v as the control input to the system instead of force F, one substitutes Eq. (1) into Eq. (5):

$$\ddot{x}_s = (1/M_s)[-d_s\dot{x}_s - k_s x_s - a\dot{\delta} - bv - n] \tag{7}$$

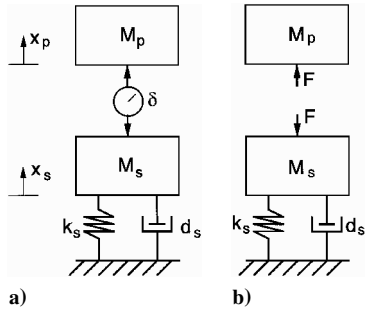

Fig. 4 Dynamic system with 2DOFs.

Similarly, Eq. (6) can be rewritten as

$$\ddot{\delta} = [(1/M_p) + (1/M_s)][a\dot{\delta} + bv + n] + (1/M_s)[d_s\dot{x}_s + k_s x_s] \quad (8)$$

Equations (7) and (8) are now in terms of the desired actuator input v. It is more convenient to express these equations in a state-space form. If the states are chosen to be $\dot{x}_s$, x_s, $\dot{\delta}$, and δ, the state-space representation of Eqs. (7) and (8) is given by

$$\begin{bmatrix} \ddot{x}_s \\ \dot{x}_s \\ \ddot{\delta} \\ \dot{\delta} \end{bmatrix} = \begin{bmatrix} -\frac{d_s}{M_s} & -\frac{k_s}{M_s} & -\frac{a}{M_s} & 0 \\ 1 & 0 & 0 & 0 \\ \frac{d_s}{M_s} & \frac{k_s}{M_s} & \frac{a}{M_p} + \frac{a}{M_s} & 0 \\ 0 & 0 & 1 & 0 \end{bmatrix} \begin{bmatrix} \dot{x}_s \\ x_s \\ \dot{\delta} \\ \delta \end{bmatrix} + \begin{bmatrix} -\frac{b}{M_s} \\ 0 \\ \frac{b}{M_p} + \frac{b}{M_s} \\ 0 \end{bmatrix} v + \begin{bmatrix} -\frac{n}{M_s} \\ 0 \\ \frac{n}{M_p} + \frac{n}{M_s} \\ 0 \end{bmatrix} \quad (9)$$

The apparently redundant state δ is needed for the output equation if displacement x_p is required. This displacement is given by

$$x_p = [0 \quad 1 \quad 0 \quad 1][\dot{x}_s \quad x_s \quad \dot{\delta} \quad \delta]^T + [0]v \quad (10)$$

The following section applies this approach to a more realistic MDOF system.

Derivation of MDOF Nonlinear Model

The full nonlinear MDOF system is more difficult to model because we are dealing with motion in all 6DOFs, which causes a complex interaction between the six actuators. The individual elements of the active module are examined in detail to ascertain the inertial forces caused by the actuator inputs.

The system is represented by Eq. (3). The left-hand side of the equation is described by a numerical model of the flexible structure, complete with the active module. The aim of this section is to derive an expression for $\boldsymbol{C_1 f_u}$, on the right-hand side of the equation, in terms of the set of control input voltages $\boldsymbol{v}$. This represents the inertial forces caused by rigid-body motion of the active module due to motion of the actuators, i.e., forces due to the control inputs.

First, expressions are derived for the rigid-body accelerations of the elements of the active module, i.e., the centroid of the platform and the six actuators. Using Newton's second law, the inertial forces are then calculated.

However, these forces are expressed in terms of the actuator input accelerations $\ddot{\boldsymbol{\delta}}$, whereas the required expression is in terms of input voltages $\boldsymbol{v}$. Hence, it is necessary to derive an expression for $\ddot{\boldsymbol{\delta}}$ in terms of $\boldsymbol{v}$. This is done by first deriving an equation for the forces in the actuators, $\boldsymbol{F}$, due to the inertial forces on the top-half of the active module. These inertial forces are caused by both rigid-body and flexible-body accelerations. Hence, an expression for $\boldsymbol{F}$ in terms of $\ddot{\boldsymbol{\delta}}$ and $\ddot{\boldsymbol{x}}$ is derived.

The forces $\boldsymbol{F}$ are also given by Eq. (1), and these two relationships can be equated to produce an expression for $\ddot{\boldsymbol{\delta}}$ in terms of $\dot{\boldsymbol{\delta}}$, $\boldsymbol{v}$, and $\ddot{\boldsymbol{x}}$. Substitution for the $\ddot{\boldsymbol{\delta}}$ term in the equation for $\boldsymbol{C_1 f_u}$ can then be made. This substitution is only valid if all of the actuators are moving, i.e., all $\dot{\delta}_i \neq 0$. If this is not the case, special expressions are obtained for the inertial forces in those actuators for which $\dot{\delta}_i = 0$, due to motion of the other actuators.

Finally, an expression for the complete system is derived, based on Eq. (3), in terms of modal parameters. This expression is represented in state-space form, using modal velocities and displacements and actuator velocities and displacements as the states of the system, with inputs $\boldsymbol{v}$.

Forces due to Control Inputs

The total force at the centroid of each element of the module consists of the inertial forces due to both rigid-body and flexible-body motion. The flexible-body forces are contained within the numerical model of the complete structure on the left-hand side of Eq. (3). The rigid-body forces are added to these forces by deriving an expression for $\boldsymbol{C_1 f_u}$ on the right-hand side of the equation.

It is assumed that the reference axes of the module remain constant with respect to the global axes, i.e., the rotation of the module due to flexible-body motion of the structure is neglected. Hence, the inertial forces due to both rigid-body motion and flexible-body motion can be superposed. The rigid-body inertial forces of the module, derived assuming the base of the module to be fixed in space, are added to the flexible-body inertial forces at the centroid of the platform (6DOF, corresponding to the three translations and three rotations) and the centroids of each actuator (3DOF, corresponding to the three translations). This simplifying assumption will introduce some inaccuracies in the dynamic model of the system, whose effects will become apparent later on.

Starting from the rigid-body forces at the centroid of the platform, the 6DOF accelerations are related to the actuator input accelerations via the Jacobian matrix. Hence, using Newton's second law of motion, the corresponding inertia forces are given by

$$\boldsymbol{f}_{u_p} = \boldsymbol{M_p}\ddot{\boldsymbol{y}} = \boldsymbol{M_p J}\ddot{\boldsymbol{\delta}} \quad (11)$$

where $\boldsymbol{M_p}$ is a matrix containing the relevant mass and centroidal moments of inertia of the platform.

Next, the forces at the centroids of the actuators, due to the rigid-body motions, are derived. Figure 5a shows that the mass of the actuator is assumed to be concentrated at its centroid. Hence, its moment of inertia is assumed to be zero. This assumption is not believed to affect significantly the accuracy of the model.

The mass of the actuator can be separated into two masses m_s and m_f, corresponding to the mass of the sliding section and the fixed part, respectively. The rigid-body accelerations $\ddot{\boldsymbol{x}}_{m_s}$ of mass m_s are given by

$$\ddot{\boldsymbol{x}}_{m_s} = \ddot{\beta}(l+\delta)\boldsymbol{e}_\theta - \dot{\beta}^2(l+\delta)\boldsymbol{e}_r + 2\dot{\beta}\dot{\delta}\boldsymbol{e}_\theta + \ddot{\delta}\boldsymbol{e}_r \quad (12)$$

where $\boldsymbol{e}_r$ and $\boldsymbol{e}_\theta$ are unit vectors, $\ddot{\beta}(l+\delta)$ is the Euler acceleration, $\dot{\beta}^2(l+\delta)$ is the centripetal acceleration, $2\dot{\beta}\dot{\delta}$ is the Coriolis acceleration, and $\ddot{\delta}$ is the relative acceleration of the mass with respect to the origin. Note that $\boldsymbol{e}_\theta$ is perpendicular to the axis of the actuator and in its current plane of motion.

Similarly, the acceleration of mass m_f is given by

$$\ddot{\boldsymbol{x}}_{m_f} = \ddot{\beta} l \boldsymbol{e}_\theta - \dot{\beta}^2 l \boldsymbol{e}_r \quad (13)$$

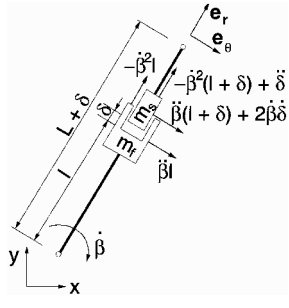

Fig. 5a Rigid-body accelerations of idealized actuator.

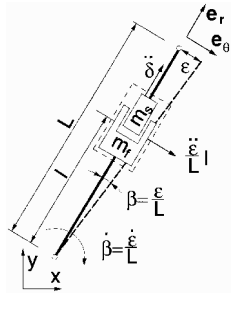

Fig. 5b Simplified rigid-body accelerations of idealized actuator.

Equations (12) and (13) can be simplified by assuming that the change in length of the actuator is small compared with its length and, hence, $(l+\delta) \simeq l$ and $(L+\delta) \simeq L$. Also, $\dot{\beta}$ and $\dot{\delta}$ are small and, hence, $\dot{\beta}^2 \simeq 0$ and $\dot{\beta}\dot{\delta} \simeq 0$. Finally, assuming that the rotation β is small, the substitution $\beta \simeq \varepsilon/(L+\delta) \simeq \varepsilon/L$ can be made and, hence, $\ddot{\beta} \simeq \ddot{\varepsilon}/L$. Here, ε is the component along $\boldsymbol{e_\theta}$ of the relative displacement between the top and bottom joints of the actuator, see Fig. 5b. It is a function of $\boldsymbol{\delta}$.

Therefore, Eqs. (12) and (13) can be reduced to

$$\ddot{\boldsymbol{x}}_{m_s} = (\ddot{\varepsilon}/L)l\boldsymbol{e_\theta} + \ddot{\delta}\boldsymbol{e_r} \tag{14}$$

$$\ddot{\boldsymbol{x}}_{m_f} = (\ddot{\varepsilon}/L)l\boldsymbol{e_\theta} \tag{15}$$

Again, applying Newton's second law, the local inertial forces f_r and f_θ, corresponding to the axial and perpendicular accelerations of the actuator, respectively, are given by

$$f_r = m_s\ddot{\delta} \tag{16}$$

$$f_\theta = (m_s + m_f)(\ddot{\varepsilon}/L)l \tag{17}$$

Introducing the matrices $\boldsymbol{H}$ and $\boldsymbol{Q}$ to transform these local forces into their components along the global axes, one obtains the global forces $\boldsymbol{f_{u_a}}$ applied to the centroids of the actuators c_{a_i}:

$$\boldsymbol{f_{u_a}} = \boldsymbol{HT}\ddot{\boldsymbol{\varepsilon}} + \boldsymbol{QS}\ddot{\boldsymbol{\delta}} \tag{18}$$

where the matrices $\boldsymbol{S}$ and $\boldsymbol{T}$ are diagonal matrices with diagonal elements $\boldsymbol{S_{ii}} = m_{s_i}$ and $\boldsymbol{T_{ii}} = (m_{s_i} + m_{f_i})l_i/L_i$, respectively, for $i = 1$–6. Substituting for $\ddot{\varepsilon}$ gives

$$\boldsymbol{f_{u_a}} = [\boldsymbol{HTUJ} + \boldsymbol{QS}]\ddot{\boldsymbol{\delta}} \tag{19}$$

The matrix $\boldsymbol{U}$ transforms the motion of the platform, $\ddot{\boldsymbol{y}} = \boldsymbol{J}\ddot{\boldsymbol{\delta}}$, into the corresponding $\ddot{\varepsilon}$.

Hence, combining the results of Eqs. (19) and (11), the complete expression $\boldsymbol{C_1 f_u}$ for the general configuration in terms of $\ddot{\boldsymbol{\delta}}$ is given by

$$\boldsymbol{C_1 f_u} = \boldsymbol{C_1}\begin{bmatrix} \boldsymbol{HTUJ} + \boldsymbol{QS} \\ \boldsymbol{M_p J} \end{bmatrix}\ddot{\boldsymbol{\delta}} = \boldsymbol{C_1 W}\ddot{\boldsymbol{\delta}} \tag{20}$$

Forces in the Actuators

Equation (20) gives an expression for $\boldsymbol{C_1 f_u}$ in terms of input accelerations $\ddot{\boldsymbol{\delta}}$. However, the desired inputs into the actuators are the voltages $\boldsymbol{v}$. Therefore, $\ddot{\boldsymbol{\delta}}$ must be replaced by $\boldsymbol{v}$, using the force–velocity–voltage relationship of Eq. (1). This can be done by establishing an expression for the forces in the actuators $\boldsymbol{F}$ in terms of the accelerations $\ddot{\boldsymbol{x}}$ and $\ddot{\boldsymbol{\delta}}$ and then replacing $\boldsymbol{F}$ by Eq. (1).

The axial forces $\boldsymbol{F}$ in the actuators are sought. These can be established by equating external and internal forces ($F = ma$) and moments ($M = I\phi$) for three axes. Hence, a set of six simultaneous equations can be formed, with the six forces $\boldsymbol{F}$ as unknowns

$$\boldsymbol{P_1 F} = [\boldsymbol{P_2}(\boldsymbol{H\tilde{T}UJ} + \boldsymbol{QS}) + \boldsymbol{P_3 M_p J}]\ddot{\boldsymbol{\delta}} + \boldsymbol{P_4}\tilde{\boldsymbol{M}}\ddot{\boldsymbol{x}} \tag{21}$$

where $\tilde{\boldsymbol{T}}_{\boldsymbol{ii}} = m_{s_i} l_i/L_i$. The matrices $\boldsymbol{P_1}$, $\boldsymbol{P_2}$, $\boldsymbol{P_3}$, and $\boldsymbol{P_4}$ resolve the forces along, or about, the appropriate axes. The matrix $\tilde{\boldsymbol{M}}$ is a diagonal matrix containing the relevant masses and mass moments of inertia associated with the platform and the actuators.

Solving Eq. (21) for the actuator forces

$$\boldsymbol{F} = \tilde{\boldsymbol{W}}\ddot{\boldsymbol{\delta}} + \boldsymbol{E}\ddot{\boldsymbol{x}} \tag{22}$$

where

$$\tilde{\boldsymbol{W}} = \boldsymbol{P_1^{-1}}[\boldsymbol{P_2}(\boldsymbol{H\tilde{T}UJ} + \boldsymbol{QS}) + \boldsymbol{P_3 M_p J}] \tag{23}$$

$$\boldsymbol{E} = \boldsymbol{P_1^{-1} P_4}\tilde{\boldsymbol{M}} \tag{24}$$

Substituting Eq. (1) for $\boldsymbol{F}$, Eq. (22) can be rearranged into

$$\ddot{\boldsymbol{\delta}} = \tilde{\boldsymbol{W}}^{-1}[(-\boldsymbol{a}\dot{\boldsymbol{\delta}} - \boldsymbol{bv} - \boldsymbol{n}) - \boldsymbol{E}\ddot{\boldsymbol{x}}] \tag{25}$$

where $\boldsymbol{a}$ and $\boldsymbol{b}$ are diagonal matrices containing scalars a_i and b_i along their diagonals, respectively, whereas $\boldsymbol{n}$ is a vector of n_i, for $i = 1$–6.

Thus, Eq. (20) can be rewritten in terms of control inputs $\boldsymbol{v}$ and actuator velocity outputs $\dot{\boldsymbol{\delta}}$:

$$\boldsymbol{C_1 f_u} = \boldsymbol{C_1 W}\tilde{\boldsymbol{W}}^{-1}[(-\boldsymbol{a}\dot{\boldsymbol{\delta}} - \boldsymbol{bv} - \boldsymbol{n}) - \boldsymbol{E}\ddot{\boldsymbol{x}}] \tag{26}$$

The substitution that leads to Eq. (25) is only valid when all $\dot{\delta}_i \neq 0$. An actuator that is not moving ($\dot{\delta}_i = 0$) behaves as a passive element and, hence, the force F_i depends on the outputs from all of the other actuators as well as the flexible body motion of the structure. It should be noted that it is possible that $\dot{\delta}_i = 0$ even when $v_i \neq 0$ because there is a dead band where the input is insufficient to overcome forces resisting motion of the actuator.

To establish values for all F_i, we must make the assumption that when $\dot{\delta}_i = 0$ then $\ddot{\delta}_i = 0$. Although this is untrue at the instant when the actuator just stops moving, it is valid while the actuator remains motionless. For the actuators that are in motion ($\dot{\delta}_i \neq 0$), Eq. (25) is used to calculate the axial accelerations of the actuators. Using these axial accelerations, the forces in all of the actuators can then be calculated from Eq. (20). The problem can be formulated as

$$\begin{bmatrix} \tilde{\boldsymbol{W}}_{11} & \boldsymbol{0} \\ \boldsymbol{W}_{21} & -\boldsymbol{I} \end{bmatrix}\begin{bmatrix} \ddot{\boldsymbol{\delta}}_{\delta\neq 0} \\ \boldsymbol{f_u} \end{bmatrix} = \begin{bmatrix} (-\boldsymbol{a_1}\dot{\boldsymbol{\delta}} - \boldsymbol{b_1 v} - \boldsymbol{n_1}) - \boldsymbol{E_1}\ddot{\boldsymbol{x}} \\ \boldsymbol{0} \end{bmatrix} \tag{27}$$

where $\tilde{\boldsymbol{W}}_{11}$ is obtained from the matrix $\tilde{\boldsymbol{W}}$ by deleting the columns and rows corresponding to $\dot{\delta}_i = 0$. Similarly, $\boldsymbol{W_{21}}$ represents the columns of matrix $\boldsymbol{W}$ corresponding to $\dot{\delta}_i \neq 0$, and $\boldsymbol{a_1}, \boldsymbol{b_1}, \boldsymbol{n_1}$, and $\boldsymbol{E_1}$ represent the rows of $\boldsymbol{a}, \boldsymbol{b}, \boldsymbol{n}$, and $\boldsymbol{E}$, respectively, corresponding to $\dot{\delta}_i \neq 0$. The vector $\ddot{\boldsymbol{\delta}}_{\delta\neq 0}$ represents the actuator accelerations corresponding to actuators for which $\dot{\delta} \neq 0$. Hence, solving Eq. (27) for $\boldsymbol{f_u}$, the equation for $\boldsymbol{C_1 f_u}$ becomes

$$\boldsymbol{C_1 f_u} = \boldsymbol{C_1 W_{21}}\tilde{\boldsymbol{W}}_{11}^{-1}[(-\boldsymbol{a_1}\dot{\boldsymbol{\delta}} - \boldsymbol{b_1 v} - \boldsymbol{n_1}) - \boldsymbol{E_1}\ddot{\boldsymbol{x}}] \tag{28}$$

State-Space Representation

Substituting Eq. (28) into Eq. (3), the equation of motion for the complete structure is given by

$$\boldsymbol{M}\ddot{\boldsymbol{x}} + \boldsymbol{D}\dot{\boldsymbol{x}} + \boldsymbol{Kx} = \boldsymbol{C_1 W_{21}}\tilde{\boldsymbol{W}}_{11}^{-1}[(-\boldsymbol{a_1}\dot{\boldsymbol{\delta}} - \boldsymbol{b_1 v} - \boldsymbol{n_1}) - \boldsymbol{E_1}\ddot{\boldsymbol{x}}] + \boldsymbol{C_2 f_{dist}} \tag{29}$$

It is more convenient to use modal approximations rather than the global mass, damping, and stiffness matrices. Hence, Eq. (29) can be altered via the modal transformation $\boldsymbol{x} = \boldsymbol{\Phi\mu}$, where $\boldsymbol{\Phi}$ is the mass normalized eigenvector matrix, to give

$$\ddot{\boldsymbol{\mu}} + 2\boldsymbol{\zeta\omega}\dot{\boldsymbol{\mu}} + \boldsymbol{\omega}^2\boldsymbol{\mu} = \boldsymbol{\Phi}^T\boldsymbol{C_1 W_{21}}\tilde{\boldsymbol{W}}_{11}^{-1} \times [(-\boldsymbol{a_1}\dot{\boldsymbol{\delta}} - \boldsymbol{b_1 v} - \boldsymbol{n_1}) - \boldsymbol{E_1}\boldsymbol{\Phi}\ddot{\boldsymbol{\mu}}] + \boldsymbol{\Phi}^T\boldsymbol{C_2 f_{dist}} \tag{30}$$

where $\boldsymbol{\omega}$ is a diagonal matrix of natural frequencies and $\boldsymbol{\zeta}$ is a diagonal matrix of damping factors.

These equations can be transformed into the following state-space form (see Ref. 7 for further details):

$$\begin{bmatrix} \ddot{\boldsymbol{\mu}} \\ \dot{\boldsymbol{\mu}} \\ \ddot{\boldsymbol{\delta}} \\ \dot{\boldsymbol{\delta}} \end{bmatrix} = \begin{bmatrix} \boldsymbol{A_1}(-2\boldsymbol{\zeta\omega}) & \boldsymbol{A_1}(-\boldsymbol{\omega}^2) & \boldsymbol{A_2 a_1} & \boldsymbol{0} \\ \boldsymbol{I} & \boldsymbol{0} & \boldsymbol{0} & \boldsymbol{0} \\ \boldsymbol{A_3}(2\boldsymbol{\zeta\omega}) & \boldsymbol{A_3}(\boldsymbol{\omega}^2) & \boldsymbol{A_4 a_1} & \boldsymbol{0} \\ \boldsymbol{0} & \boldsymbol{0} & \boldsymbol{I} & \boldsymbol{0} \end{bmatrix}\begin{bmatrix} \dot{\boldsymbol{\mu}} \\ \boldsymbol{\mu} \\ \dot{\boldsymbol{\delta}} \\ \boldsymbol{\delta} \end{bmatrix} + \begin{bmatrix} \boldsymbol{A_2 b_1} \\ \boldsymbol{0} \\ \boldsymbol{A_4 b_1} \\ \boldsymbol{0} \end{bmatrix}\boldsymbol{v} + \begin{bmatrix} \boldsymbol{A_2 n_1} \\ \boldsymbol{0} \\ \boldsymbol{A_4 n_1} \\ \boldsymbol{0} \end{bmatrix} \tag{31}$$

where

$$A_1 = \left[I + \Phi^T C_1 W_{21} \tilde{W}_{11}^{-1} E_1 \Phi\right]^{-1} \tag{32}$$

$$A_2 = \left[I + \Phi^T C_1 W_{21} \tilde{W}_{11}^{-1} E_1 \Phi\right]^{-1} \left(-\Phi^T C_1 W_{21} \tilde{W}_{11}^{-1}\right) \tag{33}$$

$$A_3 = W^{-1} W_{21} \tilde{W}_{11}^{-1} E_1 \Phi^T \left[I + \Phi^T C_1 W_{21} \tilde{W}_{11}^{-1} E_1 \Phi\right]^{-1} \tag{34}$$

$$A_4 = W^{-1} W_{21} \tilde{W}_{11}^{-1} \times \left[I + E_1 \Phi^T \left(I + \Phi^T C_1 W_{21} \tilde{W}_{11}^{-1} E_1 \Phi\right)^{-1} \Phi^T C_1 W_{21} \tilde{W}_{11}^{-1}\right] \tag{35}$$

Assuming that the measured outputs $\boldsymbol{y}$ are the rotations and displacements of the centroid of the platform, the output expression is given by

$$\boldsymbol{y} = [\boldsymbol{0} \quad V\Phi \quad \boldsymbol{0} \quad \boldsymbol{J}][\dot{\mu} \quad \mu \quad \dot{\delta} \quad \delta]^T + [\boldsymbol{0}]\boldsymbol{v} \tag{36}$$

where $\boldsymbol{V}$ extracts the relevant flexible-body displacements and rotations for the platform centroid from the vector of generalized displacements.

These state equations can be implemented numerically in a discretized form. However, it must be noted that the values for a_i, b_i, and n_i change depending on the direction of movement of each actuator, i.e., the sign of $\dot{\delta}_i$. Therefore, for each cycle of the simulation, it is necessary establish, iteratively, whether or not the input voltage is great enough to overcome the internal forces in the actuator and, thus, sufficient to initiate or continue motion in the desired direction. Further implementation details can be found in Ref. 7.

Linearized Model

To apply relatively straightforward and well-developed modern linear control design techniques, a linear model of the system is desirable. The nonlinear relationship between actuator force, velocity, and voltage is represented by Eq. (1). To linearize this relationship, the effects of inertial forces on the actuators are ignored. Provided the levels of excitation due to force inputs remain low, this is an acceptable approximation. Hence, the actuator relationship can now be represented by two straight lines, instead of two planes, separated by a dead band. The equation for each line is given by

$$v_i = \tilde{a}_i \dot{\delta}_i + \tilde{n}_i \tag{37}$$

where $\tilde{a} = (a/b)$ and $\tilde{n} = (n/a)$. Thus, we can now produce a linear model with velocity $\dot{\delta}_i$ as the input. The voltage v_i required to produce the required velocity can be estimated, in a separate calculation, using Eq. (37), the coefficients of which will depend on the sign of the velocity.

The modal equation of motion for the continuous system, with a disturbance input, is given by

$$\ddot{\mu} + 2\zeta\omega\dot{\mu} + \omega^2\mu = \Phi^T C_1 W \ddot{\delta} + \Phi^T C_2 f_{\text{dist}} \tag{38}$$

By defining a new state η, we can produce a model with input $\dot{\delta}$, where η is a linear combination of the system variables, given by

$$\eta = \dot{\mu} - \Phi^T C_1 W \dot{\delta} \tag{39}$$

Hence, from Eq. (38), we get

$$\dot{\eta} = -2\zeta\omega\eta - 2\zeta\omega\Phi^T C_1 W \dot{\delta} - \omega^2\mu + \Phi^T C_2 f_{\text{dist}} \tag{40}$$

The equation of motion is now in terms of the states η and μ, with control inputs $\dot{\delta}$ and disturbance input f_{dist}. Thus, the model of the system is given by

$$\begin{bmatrix} \dot{\eta} \\ \dot{\mu} \end{bmatrix} = \begin{bmatrix} -2\zeta\omega & -\omega^2 \\ I & 0 \end{bmatrix} \begin{bmatrix} \eta \\ \mu \end{bmatrix} + \begin{bmatrix} -2\zeta\omega\Phi^T C_1 W & \Phi^T C_2 \\ \Phi^T C_1 W & 0 \end{bmatrix} \begin{bmatrix} \dot{\delta} \\ f_{\text{dist}} \end{bmatrix} \tag{41}$$

As for the nonlinear case, for the purposes of representing the displacement and rotation output of the system, additional states δ must be added to the model:

$$\boldsymbol{y} = [\boldsymbol{0} \quad V\Phi \quad \boldsymbol{J}] \begin{bmatrix} \eta \\ \mu \\ \delta \end{bmatrix} + [\boldsymbol{0} \quad \boldsymbol{0}] \begin{bmatrix} \dot{\delta} \\ f_{\text{dist}} \end{bmatrix} \tag{42}$$

Quasistatic Control

The quasistatic control problem involves correction for misalignment of the active module platform while quasistatic disturbances are applied to the flexible structure. The shape of the flexible structure itself is not altered by the control inputs, but the error between the disturbed position of the module platform and the desired position is removed by the active module. The active module allows correction for all 6DOFs. The aim is to design a controller that will allow the correction of these disturbances without exciting flexible structural modes, resulting in instability.

Assuming the base of the module to be fixed, the relationship between the position error of the platform $\boldsymbol{y}$ and the required change in length of the actuators δ is provided by the Jacobian matrix

$$\delta = \boldsymbol{J}^{-1}\boldsymbol{y} \tag{43}$$

However, this is only an approximation because the base of the module moves, due to disturbances. It is only through the use of feedback of the absolute position $\boldsymbol{y}$ that the position error can be corrected for. Hence, using the relationship given by Eq. (43), a simple proportional controller can be formed. A negative feedback controller that relates the velocity inputs $\dot{\delta}$ proportionally to the error in the length of the actuators δ is desired:

$$\dot{\delta} = -\boldsymbol{C_p}\delta = -\boldsymbol{C_p}\boldsymbol{J}^{-1}\boldsymbol{y} \tag{44}$$

where $\boldsymbol{C_p}$ is the diagonal gain matrix, to be chosen.

Because of the symmetry of both the module and the structure, it is reasonable for the controller gain for all actuators to be the same. Therefore, the diagonal gain matrix $\boldsymbol{C_p}$ can be replaced by a single value c_p. [Note that the equal gains chosen for the actuators are weighted by $\boldsymbol{J}^{-1}$ in Eq. (44) and, hence, do not correspond to equal gains for all DOFs.] It is simple to show that a high-gain controller will reject disturbances better than a low-gain controller. However, because the controller is based entirely on a kinematic relationship, with the flexible-body dynamics ignored, the system may become unstable.

The control inputs $\dot{\delta}$ are, in reality, related to the actuator positions δ by both $\boldsymbol{J}^{-1}$ and $\boldsymbol{G}(\boldsymbol{s})$, the dynamics of the open-loop system. Hence, the position output of each actuator is coupled to the velocity inputs of all six actuators and, therefore, a multi-input/multi-output stability analysis, such as the generalized Nyquist stability criterion, is required.[8] Thus, a plot of the characteristic loci of $\boldsymbol{G}(\boldsymbol{s})\boldsymbol{J}^{-1}$ for the linear model shows that the system remains stable for controller gains $0 < c_p < 6.2$. For $c_p > 6.2$, the system may become unstable.[9]

These conclusions have been verified by numerical simulations based on the nonlinear model. Typical results are shown in Figs. 6 and 7 for controller gains of $c_p = 6$ and 8. An initial offset in the position of the system was applied, and then the time response of the system was simulated, with the controller switched on after 0.5 s. Only the first 4 s of the simulation are shown, as nothing unexpected happened after that.

For $c_p = 6$, the error reduces quickly in the initial stages, slowing down as the error approaches zero. It is evident from Fig. 6 that, although a small amount of vibration is introduced into the system, it is insufficient to cause instability. However, for a gain of $c_p = 8$, as shown in Fig. 7, the system clearly becomes unstable, as predicted.

Tests on the actual structure were also performed. Figure 8 shows the response for a controller gain of $c_p = 6$. Comparing the simulation to the measured results, for translational behavior the agreement is remarkably accurate; however, the rotations of the simulated structure are faster than those of the real structure. It is believed that this is an effect of having simplified the calculation of the inertia forces, in the previous section titled "Forces due to Control Inputs." The (small) residual offsets are a result of using Eq. (1) to linearize

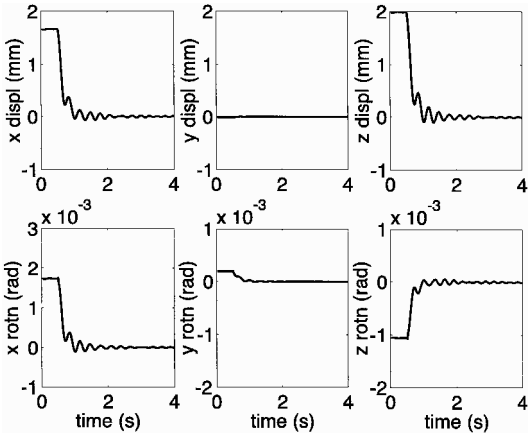

Fig. 6 Simulated time response for closed-loop system with proportional controller gain, $c_p = 6$.

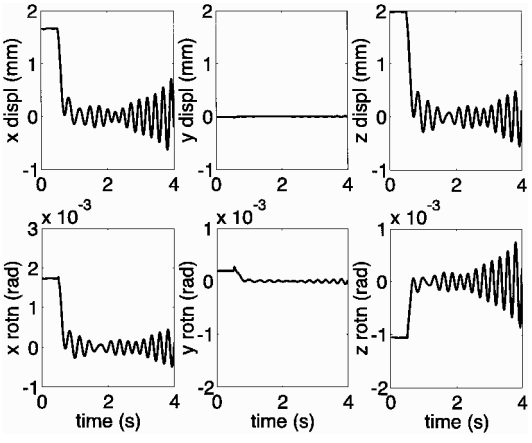

Fig. 7 Simulated time response for closed-loop system with proportional controller gain, $c_p = 8$.

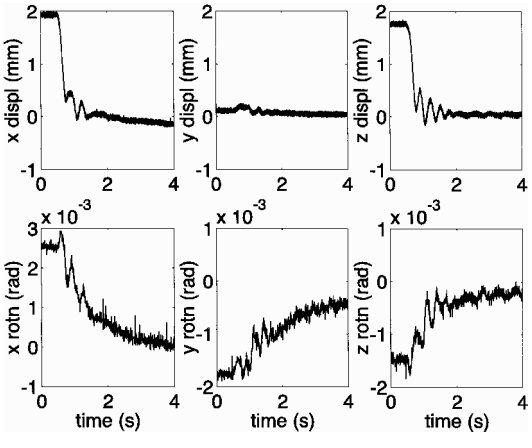

Fig. 8 Measured time response for closed-loop system with proportional controller gain, $c_p = 6$.

the typical actuator response of Fig. 2. A controller gain of $c_p = 8$ produced unstable behavior.[7] Hence, the generalized Nyquist stability criterion appears to give a good estimate of the instability of the system without the need for complex nonlinear analysis.

To demonstrate the ability of the controller to maintain the position of the platform despite the effects of quasistatic disturbances, a number of tests were performed. The tests involved the comparison of the open-loop and closed-loop response of the system to a random disturbance input, achieved through the heating of various structural members. The open-loop time response for a disturbance input is shown by the dotted line in Fig. 9, for each DOF. Displacements greater than ± 1 mm and rotations of ± 0.001 rad occur. The

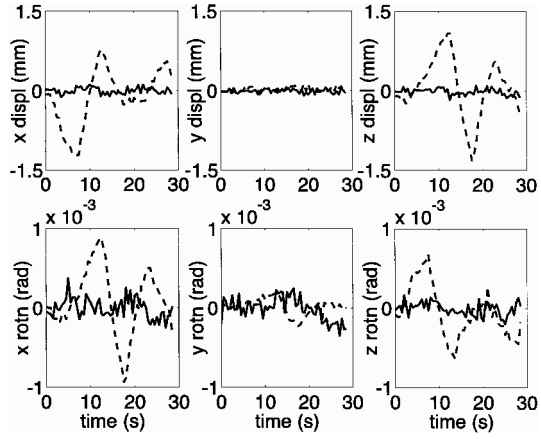

Fig. 9 Measured response to a quasistatic disturbance input.

y displacement and the corresponding rotation of the platform are negligible because the input does not easily allow these motions.

To control the disturbances, the proportional controller with a gain of six was used, which allows good disturbance rejection without causing instability. The closed-loop time response, for the same random disturbance sequence, is shown by the solid line in Fig. 9. The motion of the platform is kept within approximately ± 0.1 mm and ± 0.00025 rad. This is typical of the measured results for all disturbance inputs tested, even for larger amplitude disturbances. Most of the measured response consists of sensor noise.

The precision with which the position of the platform may be maintained is largely due to the accuracy of the linear variable-voltage displacement transformer sensors, whose resolution was approximately 0.1 mm. It seems reasonable, because the actuators are designed to have a resolution of the order of micrometers, that a greater precision would be possible if the sensor noise and resolution were improved.

Vibration Control

The vibration control problem involves the design of a controller to counteract the effects of dynamic disturbances. Controllers can be designed using the linearized model of the system as in the preceding section, but, because in vibration control the forces induced in the actuators by the inertia of the platform may be significant, it is essential to examine the stability of the controllers, as well as their performance, through the use of the nonlinear simulation.

Initially an optimal LQG-Kalman filter controller was designed to reduce the effect of dynamic disturbances on the payload.[7,9] However, it was found that, to provide a reasonable stability margin, the performance of the controller had to be compromised.

The Glover–McFarlane H_∞ loop-shaping design procedure[10,11] is a simple method allowing performance and robust stability trade-offs, with a guarantee of some degree of closed-loop stability. The loop-shaping method uses a precompensator and/or a postcompensator to shape the nominal open-loop system to give the desired open-loop shape. A stabilizing controller is then synthesized by minimizing the closed-loop gains from disturbances to the inputs and outputs of the shaped system.

A controller was designed for the test system by trading off performance and stability requirements. A reasonable stability margin was allowed to take the effects of nonlinearities into account, and the controller gain was monitored to prevent actuator saturation. Tests were performed by applying a constant sinusoidal disturbance input to the flexible structure, corresponding to the first natural frequency of the system. The controller was switched on after 2 s. The closed-loop time response plots for the nonlinear simulation are shown in Fig. 10. A reduction by a factor of approximately two is estimated for the in-plane displacements, with a greater reduction by a factor of approximately eight for the corresponding rotational DOFs. The y displacement and rotation show behavior caused by the actuator nonlinearities.

The measured response, shown in Fig. 11, corresponds well with the simulated response. The reduction in levels of vibration are

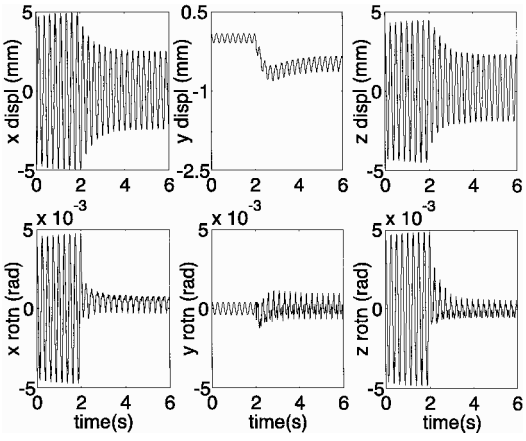

Fig. 10 Nonlinear simulation of closed-loop time response for H_∞ loop-shaping controller.

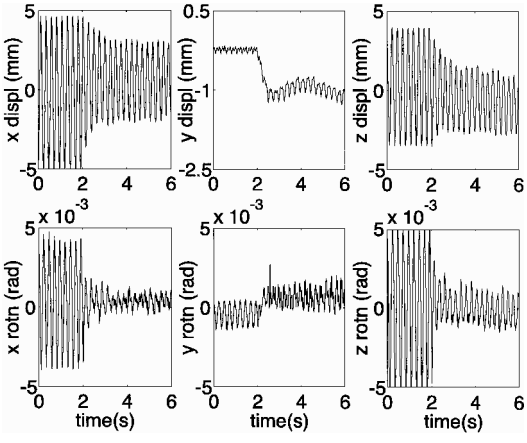

Fig. 11 Measured closed-loop time response for H_∞ loop-shaping controller

similar to those estimated, and the system remains stable, despite noise and uncertainties, although the performance is slightly less than expected. A higher degree of control may be possible through further design iterations.

Conclusions

A 6DOF system of actuators has been designed to control the effects of both large amplitude quasistatic disturbances and vibration disturbances. The actuators are arranged to form a Stewart platform, which is attached to the tip of a flexible mast. To adequately perform both functions using the same hardware, a new type of long-stroke inertial slip-stick actuator is used. Nonlinear features of the actuator have been assessed and modeled.

A nonlinear system of equations has been developed to predict the performance and stability of the controlled dynamic system. This is achieved through substitution of an experimentally derived actuator model into the equation of motion of the structure. A simplified model has also been derived to allow the application of linear control theory.

Quasistatic control has been achieved simply by using a proportional controller. Stability of the controller has been assessed using the generalized Nyquist stability criterion. Simulations and measurements have shown that this produces a good estimate of stable regions. Disturbances of the order of millimeters have been controlled to within 0.1 mm, which is the same order as the sensor noise.

A vibration controller has been designed based on the linearized dynamic model. The H_∞ loop-shaping procedure has been used to design a simple controller, which minimizes the effect of disturbances on the input and output, guaranteeing some degree of stability margin. Because of saturation limits of the actuator, the performance of the system was limited. However, results of the nonlinear simulation and the measured results correspond quite well, demonstrating the validity of assumptions made to develop the nonlinear model.

Acknowledgments

We gratefully acknowledge financial support toward the work presented provided by the Engineering and Physical Sciences Research Council, The Royal Society of London, and Matra–Marconi Space U.K. We are also grateful to G. W. Game and C. J. H. Williams, formerly at British Aerospace Space Systems and to our colleague K. Glover for their advice and encouragement during the course of this work. Helpful comments by the reviewers have been incorporated in the final version of this paper.

References

[1]Stewart, D., "A Platform with Six Degrees of Freedom," *Proceedings of the Institution of Mechanical Engineers*, Vol. 180, No. 15, 1965, pp. 371–378.

[2]Geng, Z. J., and Haynes, L. S., "Six Degree of Freedom Active Vibration Control Using the Stewart Platform," *IEEE Transactions on Control Systems Technology*, Vol. 2, No. 1, 1994, pp. 45–53.

[3]Spanos, J., Rahman, Z., and Blackwood, G., "A Soft 6-Axis Active Vibration Isolator," American Control Conference, Seattle, WA, 1995, pp. 412–416.

[4]Tanaka, M., and Hanahara, K., "Stochastic Approach to Static Control of Adaptive Truss Under Imperfection of Adjustable Member Lengths," Second Joint Japan/U.S. Conference on Adaptive Structures, Nagoya, Japan, 1991, pp. 406–418.

[5]Darby, A. P., and Pellegrino, S., "Inertial Stick-Slip Actuator for Active Control of Shape and Vibration," *Journal of Intelligent Materials, Systems and Structures*, Vol. 8, No. 12, 1997, pp. 1001–1011.

[6]You, Z., and Pellegrino, S., "Cable-Stiffened Pantographic Deployable Structures Part 1: Triangular Mast," *AIAA Journal*, Vol. 34, No. 4, 1996, pp. 813–820.

[7]Darby, A. P., "Active Control of Flexible Structures Using Inertial Slip-Stick Actuators," Ph.D. Dissertation, Cambridge Univ., Cambridge, England, UK, 1996.

[8]Maciejowski, J. M., *Multivariable Feedback Design*, Addison–Wesley, Reading, MA, 1989.

[9]Darby, A. P., and Pellegrino, S., "Active Alignment Control of a Payload Using Non-Linear, Long-Stroke Actuators," *Proceedings of the IUTAM Symposium on Interaction Between Dynamics and Control in Advanced Mechanical Systems*, edited by D. H. van Campen, Kluwer, Dordrecht, The Netherlands, 1997, pp. 91–100.

[10]McFarlane, D., and Glover, K., "A Loop Shaping Design Procedure Using H_∞ Synthesis," *IEEE Transactions on Automatic Control*, Vol. 37, No. 6, 1992, pp. 759–769.

[11]Balas, G. J., Doyle, J. C., Glover, K., Packard, A., and Smith, R., "μ-Analysis and Synthesis Toolbox User's Guide," The MathWorks, Inc., Natick, MA, 1993.